**Supplementary Material (ESI)**

# A novel 3D Zn-coordination polymer based on a multiresponsive fluorescent sensor demonstrating outstanding sensitivities and selectivities for the efficient detection of multiple analytes

Yu Liu,[a] Yan Wang,[a] Xiao-Sa Zhang,[a] Yu-Shu Sheng,[a] Wen-Ze Li,[a*] Ai-Ai Yang,[a] Jian Luan,[b*] Hong-Zhu Liu[c] and Zhong-Gang Wang[d]

[a] *College of Science, Shenyang University of Chemical Technology, Shenyang, 110142, P. R. China*

[b] *College of Sciences, Northeastern University, Shenyang, 100819, P. R. China*

[c] *Post-Doctoral Research Station of Dalian Zhenbang Fluorocarbon Paint Stock Co., Ltd., Dalian, 116036, P. R. China*

[d] *State Key Laboratory of fine Chemicals, Department of Polymer Science and Materials, School of Chemical Engineering, Dalian University of Technology, Dalian, 116024, P. R. China*

**Table S1.** Crystallographic data for complex **1**.

| Complex | **1** |
|---|---|
| Empirical formula | $C_{34}H_{34}N_4Zn_2O_{14}$ |
| Formula weight | 853.39 |
| Crystal system | Monoclinic |
| Space group | *P21/n* |
| *a* (Å) | 8.8708(5) |
| *b* (Å) | 28.9726(15) |
| *c* (Å) | 13.5048(7) |
| *α* (°) | 90 |
| *β* (°) | 91.9020(10) |
| *γ* (°) | 90 |
| *V* (Å $^3$) | 3469.0(3) |
| *Z* | 4 |
| $D_c$ (g cm$^{-3}$) | 1.634 |
| $R_{int}$ | 0.0284 |
| GOF | 1.008 |
| $R_1{}^a$ [$I > 2\sigma(I)$] | 0.0358 |
| $wR_2{}^b$ (all data) | 0.0519 |

[a] $R_1 = \Sigma||F_o|-|F_c||/\Sigma|F_o|$, [b] $wR_2 = \Sigma[w(F_o^2-F_c^2)^2]/\Sigma[w(F_o^2)^2]^{1/2}$.

**Table S2** Selected bond distances (Å) and angles (°) for complex **1**.

| | | | |
|---|---|---|---|
| Zn(1)–O(1W) | 1.9695(17) | Zn(2)–O(7)#1 | 1.9581(16) |
| Zn(1)–O(4) | 1.9734(16) | Zn(2)–O(3) | 2.0109(15) |
| Zn(1)–O(1) | 1.9748(17) | Zn(2)–N(4)#2 | 2.0341(18) |
| Zn(1)–N(1) | 2.0496(19) | N(4)–Zn(2)#4 | 2.0341(18) |
| Zn(2)–O(5) | 1.9574(17) | O(7)–Zn(2)#5 | 1.9581(16) |
| O(1W)–Zn(1)–O(4) | 102.05(7) | O(5)–Zn(2)–O(7)#1 | 100.42(8) |
| O(1W)–Zn(1)–O(1) | 105.07(7) | O(5)–Zn(2)–O(3) | 116.94(7) |
| O(4)–Zn(1)–O(1) | 133.80(7) | O(7)#1–Zn(2)–O(3) | 96.15(7) |
| O(1W)–Zn(1)–N(1) | 102.48(7) | O(5)–Zn(2)–N(4)#2 | 111.84(8) |
| O(4)–Zn(1)–N(1) | 100.94(7) | O(7)#1–Zn(2)–N(4)#2 | 130.34(8) |
| O(1)–Zn(1)–N(1) | 108.68(8) | O(3)–Zn(2)–N(4)#2 | 101.22(7) |

Symmetry codes: #1 $x + 1/2, -y + 1/2, z - 1/2$; #2 $-x + 1/2, y - 1/2 -z + 1/2$; #4 $-x + 1/2, y + 1/2, -z + 1/2$; #5 $x - 1/2, -y + 1/2, z + 1/2$.

**Table S3** List of CPs utilized in the sensing of $Mg^{2+}$ in water.

| CP | Detection limit | Reference |
|---|---|---|
| Boron-doped carbon dots (BCDs) | 39 μM | S1 |
| $[Zn_2(3\text{-bpah})(bpta)(H_2O)]\cdot 3H_2O$ | 10 μM | This work |
| 8-hydroxyquinoline-5-benzothiazole (QB) | $1.40\times10^{-1}$ μM | S2 |
| Quinoline-based fluorescent probe (QC) | $6.28\times10^{-2}$ μM | S3 |
| $[Ln(BIPA\text{-}TC)_{0.5}(DMA)_2(NO_3)]\cdot DMA\cdot H_2O$ $H_4BIPA\text{-}TC$=tetra-carboxylate ligand | $1.53\times10^{-4}$ μM | S4 |

**Table S4** List of CPs utilized in the sensing of $Cr_2O_7^{2-}$ in water.

| CP | Detection limit | Reference |
|---|---|---|
| $[Zn_4(3\text{-dpyb})_2(odpa)_2(H_2O)_3]\cdot 4H_2O$ | 41.50 μM | S5 |
| $\{[Zn_2(L_2)_2(H_2O)_4]\cdot H_2O\}$ | 2.60 μM | S6 |
| $[Zn_2(TPOM)(NH_2\text{-}BDC)_2]\cdot 4H_2O$ | 3.90 μM | S7 |
| $[Zn(DDB)(DPE)]\cdot H_2O$ | 0.64 μM | S8 |
| $[Zn_2(3\text{-bpah})(bpta)(H_2O)]\cdot 3H_2O$ | $1.00\times10^{-3}$ μM | This work |

**Table S5**. Comparison of the overlap between complex **1** and various analytes.

| CP | Analyte overlap | Reference |
|---|---|---|
| $[Zn_4(\mu_3\text{-}OH)_2(BTC)_2(BBI4PY)_2]\cdot 10H_2O$ | $Fe^{3+}$, TNP | S9 |
| g-CNQDs@Zn-MOF<br>g-CNQDs = graphitic carbon nitrides quantum dots | riboflavin (RF) | S10 |
| $[Zn_2(NDC)_2(bpy)]\cdot G_x$<br>NDC = 2,6-naphthalenedicarboxylic acid,<br>bpy = 4,40-bipyridine, G=guest solvent molecules | Nitroaromatics | S11 |
| $[Zn(OPE)\cdot 2H_2O]$<br>OPE = oligo-phenyleneethynylene-dicarboxylic | DSMP | S12 |
| $[Zn_2(NDC)_2(DPTTZ)]$<br>NDC = naphthalene dicarboxylate<br>DPTTZ = *N*,*N*′-di(4-pyridyl)thiazolo-[5,4-d]thiazole | $Hg^{2+}$ | S13 |
| $[Zn_3(bpg)_{1.5}(azdc)_3]\cdot(DMF)_{5.9}\cdot(H_2O)_{1.05}$ | $Fe^{3+}$, NZF, TNP | S14 |
| $[Zn_3(DDB)(DPE)]\cdot H_2O$<br>H5DDB = 3,5-di(2′,4′-dicar-boxylphenyl)benzoic acid<br>DPE = 1,2-di(4-pyridyl)ethylene) | $Fe^{3+}$, $Cr^{3+}$, $Cr_2O_7^{2-}$, $CrO_4^{2-}$, $MnO_4^-$, 2,6-Dich-4-NA) | S15 |
| $[Zn_2(IDS)(bipy)_{1.5}]$<br>$H_4IDS$ = meso-iminodisuccinic acid<br>bipy = 4,4-bipyridine | $Fe^{3+}$, TNP | S16 |
| $[Zn(TIPA)(NO_3))_2(H_2O)]\cdot 5H_2O$<br>TIPA = tri(4-imidazolylphenyl)amine | TNP, 4-NP, RDX, HMX, DMNB | S17 |
| $[Zn(QDA)]\cdot 0.5H_2O\cdot 0.7DMF$<br>$H_2QDA$ = quinoline-2,6-dicarboxylic acid | $Fe^{3+}$ | S18 |

| | | |
|---|---|---|
| Zn(DMA)(TBA)<br>$H_2$TBA = 4-(1H-tetrazol-5-yl)-benzoic acid | $Al^{3+}$, NACs | S19 |
| $(Zn_2(DHBDC)(DMF)(H_2O)_2$<br>$H_4$dondc = 1,5-dioxido-2,6-naphthalenedicarboxylic acid | TBBPA | S20 |
| $[Zn_4(L^{3-})_2(O^{2-})(H_2O)_2]\cdot 4EtOH\}_n$/Tb@Zn-MOF<br>$H_3L$ = 4,4′,4″-[(1,3,5-triazine-2,4,6-triyl)tris-(sulfanediyl)]tribenzoic acid | $PO_4^{3-}$ | S21 |
| $[Zn_2(4\text{-bpft})_2(1,3\text{-BDC})_2]\cdot 2H_2O$<br>[Zn(4-bpft)(5-MIP)]<br>[Zn(4-bpft)(5-HIP)]<br>4-bpft = *N*,*N*′-bis(4-pyridine formamide)-3,4-thiophene<br>1,3-$H_2$BDC = isophthalic acid<br>5-$H_2$MIP = 5-methylisophthalic acid<br>$H_2$HIP = 5-hydroxyisophthalic acid | $Hg^{2+}$, Purines | S15 |
| $[Zn_4(3\text{-dpyb})_2(odpa)_2(H_2O)_3]\cdot 4H_2O$ | $Fe^{3+}$, $Cr_2O_7^{2-}$, $MnO_4^-$ | S22 |
| $[Zn(tptc)_{0.5}(bpy)(H_2O)]$<br>bpy = 2,2′-bipyridine, $H_4$tptc = *p*-terphenyl-2,2″,5″,5‴-tetracarboxylate acid | $Cr_2O_7^{2-}$ | S23 |
| $[Zn_8(ad)_4(BPDC)_6\cdot 2Me_2NH_2\cdot 8DMF\cdot 11H_2O]$<br>ad = adeninate<br>BPDC = biphenyldicarboxylate | $Fe^{3+}$, $Al^{3+}$, $Cr_2O_7^{2-}$ | S24 |
| $[Zn_2(3\text{-bpah})(bpta)_2(H_2O)]\cdot 3H_2O$ | $Fe^{3+}$, $Mg^{2+}$, $Cr_2O_7^{2-}$, $MnO_4^-$, NB, NM | This work |

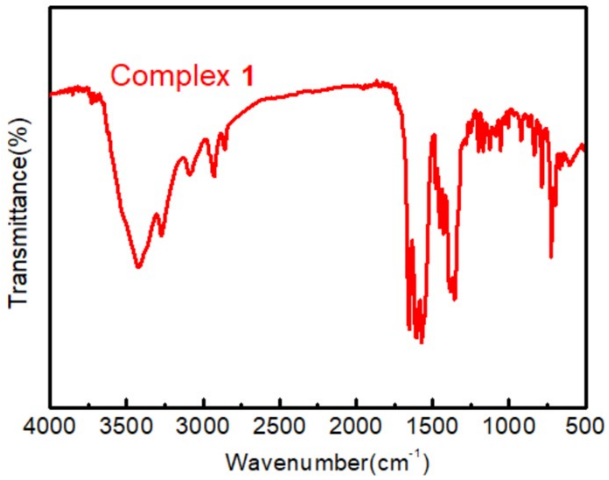


**Fig. S1** The IR spectrum of complex **1**.

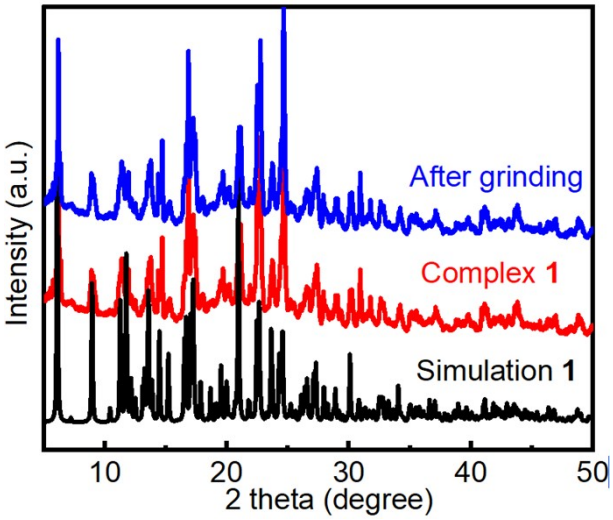


**Fig. S2** The powder X–ray diffraction patterns of simulated **1**, fresh sample **1** and complex **1** after grinding.

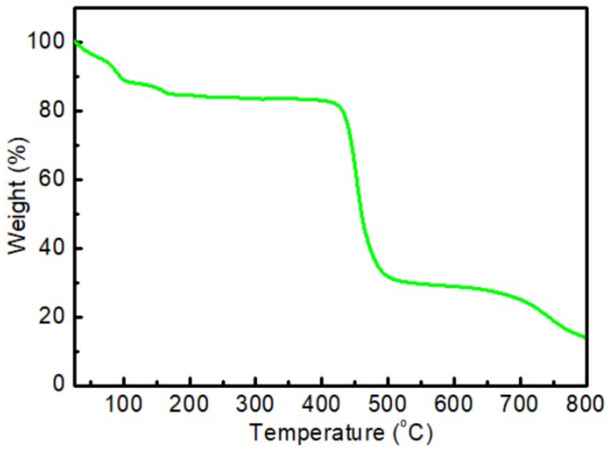


**Fig. S3** The TG curve of complex **1**.

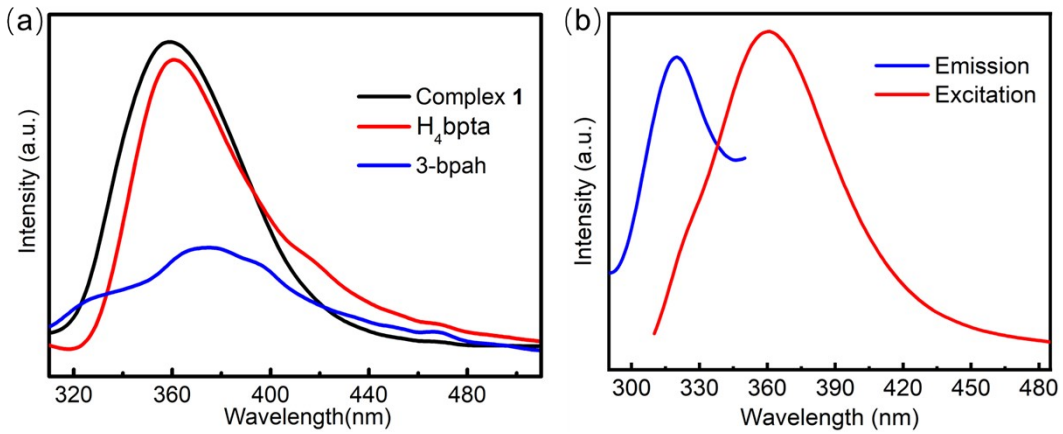


**Fig. S4** The emission spectra of complex **1**, $H_4$bpta and 3-bpah in the solid state. (b) The solid excitation and emission spectra of **1**.

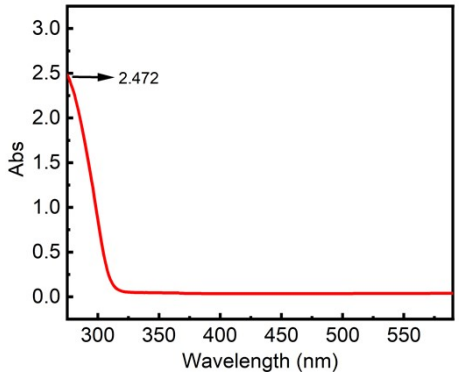


**Fig. S5** UV-Vis adsorption spectrum of the suspension of **1**.

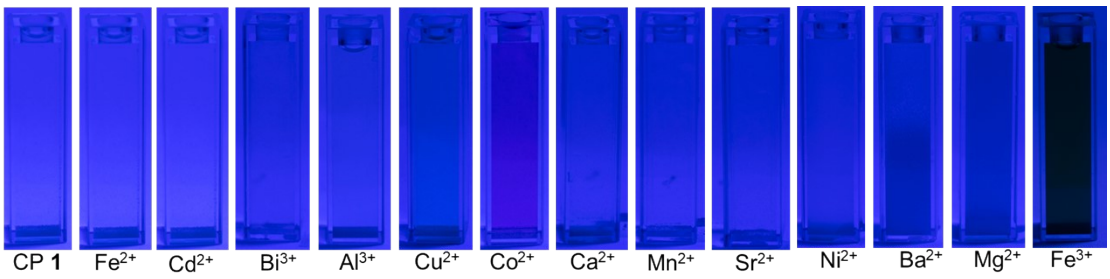


**Fig. S6** Fluorometric pictures with various metal ions.

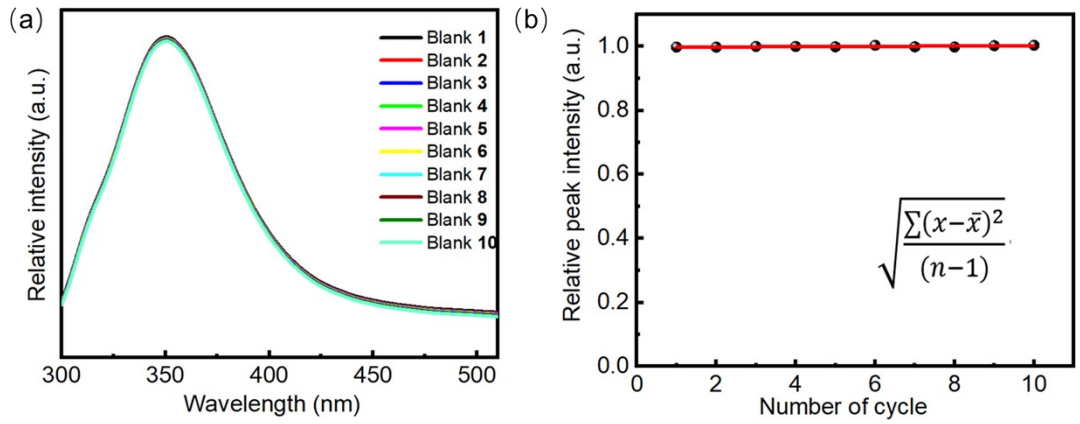


**Fig. S7** The photoluminescence spectra from ten cycles blank measurements for solid state of **1**. (b) Calibration curve with blank measurements after ten cycles (insert: the standard deviation formula, where, and represent the luminescence intensity values of **1** after normalization, the average of the maximum luminescence intensity values of **1** after ten cycles and the cycles of blank measurements, respectively). The luminescence intensity values of **1** after normalization: 0.9979, 0.9977, 1.0002, 0.9996, 0.9989, 1.0035, 0.9989, 0.9983, 1.0023, 1.0036. Calculated standard deviation, $\delta = 0.003887$.

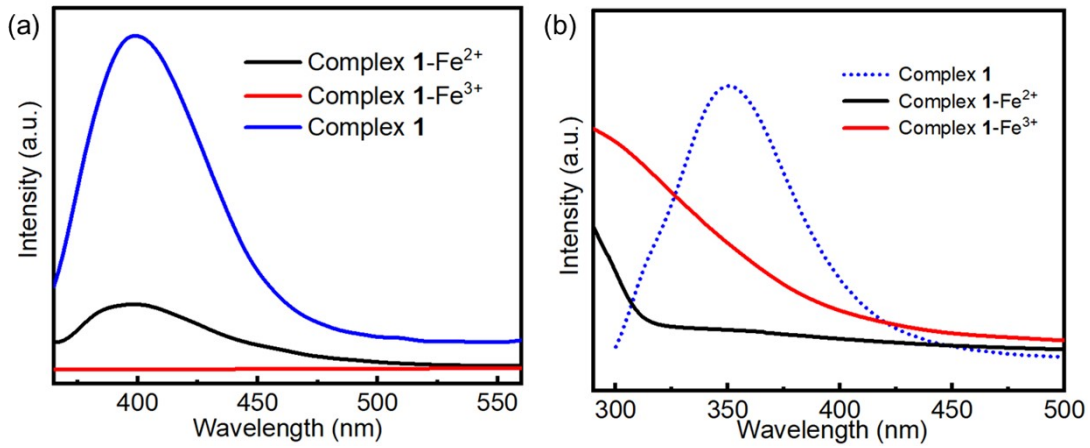


**Fig. S8** (a) The emission spectra of complex **1**, **1**-$Fe^{2+}$ and **1**-$Fe^{3+}$; (b) UV-Vis adsorption spectra of **1**-$Fe^{2+}$ and **1**-$Fe^{3+}$ along with the emission spectrum of **1**.

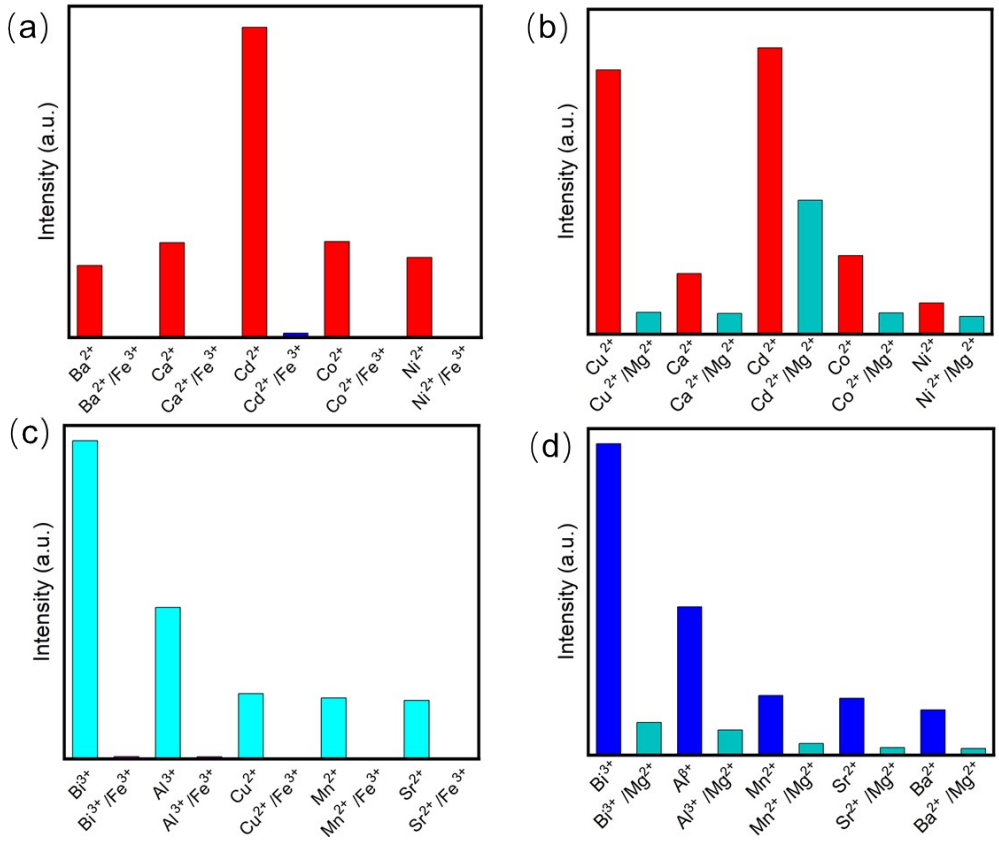


**Fig. S9** The effect of adding other metal cations on the luminescence intensity of $Fe^{3+}$ (0.1 M) and $Mg^{2+}$ cations (0.1 M).

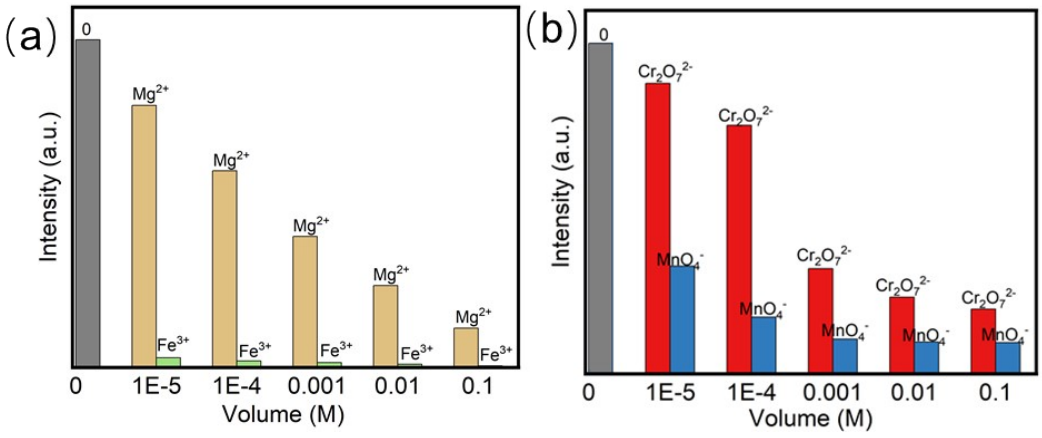


**Fig. S10** (a) Fluorescence spectra of competitive quenching of $Fe^{3+}$ and $Mg^{2+}$; (b) Fluorescence spectra of competitive quenching of $MnO_4^-$ and $Cr_2O_7^{2-}$.

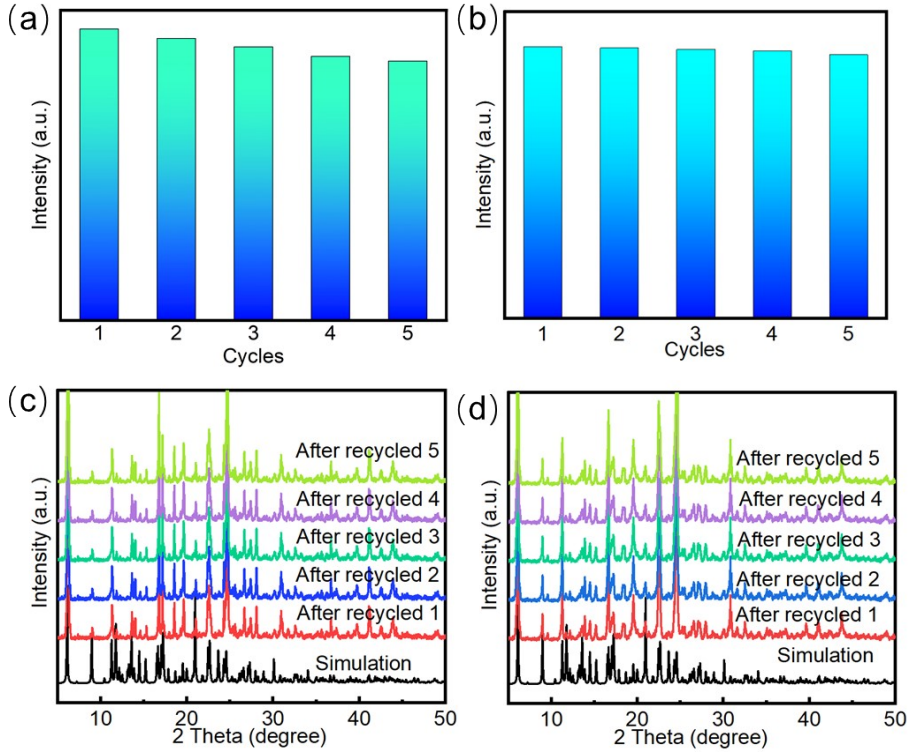


**Fig. S11** The cyclic response of the luminescence intensities of **1** for detecting $Fe^{3+}$ (a) and $Mg^{2+}$ (b); The PXRD patterns of **1** treated by the $Fe^{3+}$ (c), and $Mg^{2+}$ (d).

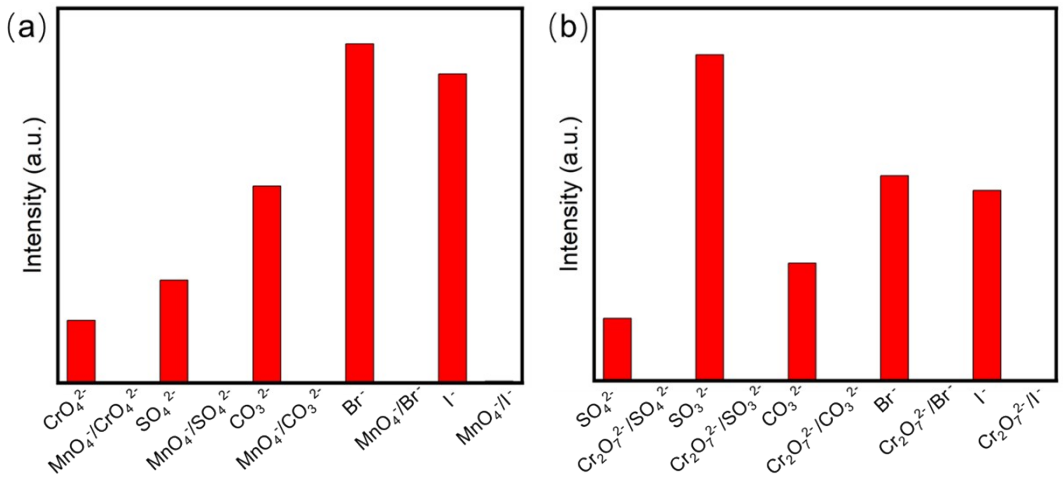


**Fig. S12** The effect of adding other metal cations on the luminescence intensity of $MnO_4^-$ (0.1 M) and $Cr_2O_7^{2-}$ cations (0.1 M).

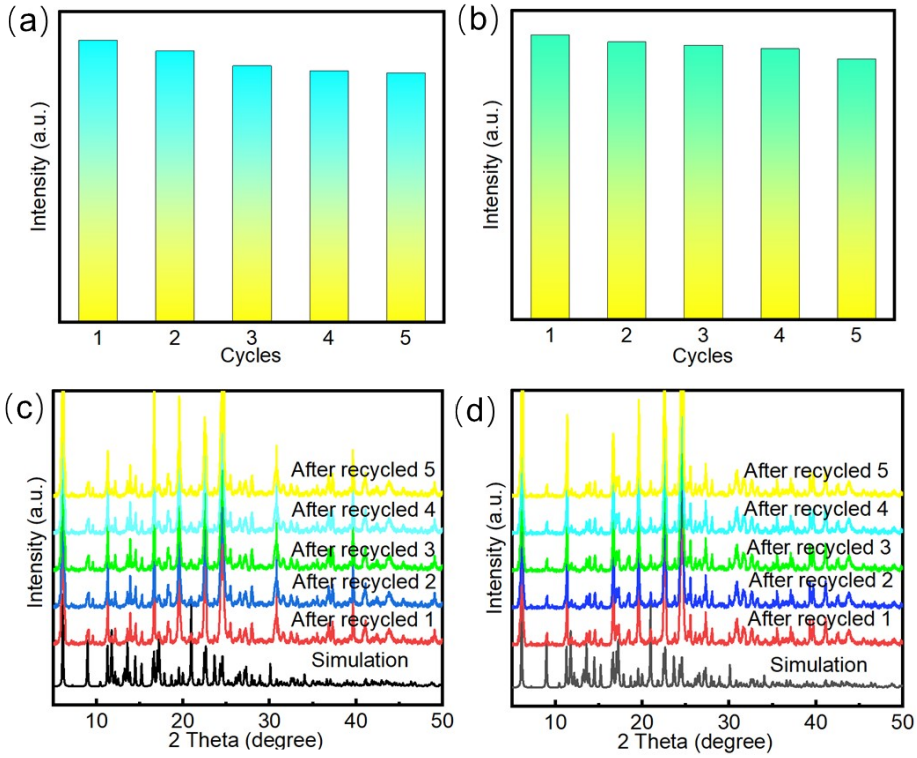


**Fig. S13** The cyclic response of the luminescence intensities of **1** for detecting $Cr_2O_7^{2-}$ (a) and $MnO_4^-$ (b); The PXRD patterns of **1** treated by the $Cr_2O_7^{2-}$(c), and $MnO_4^-$ (d)

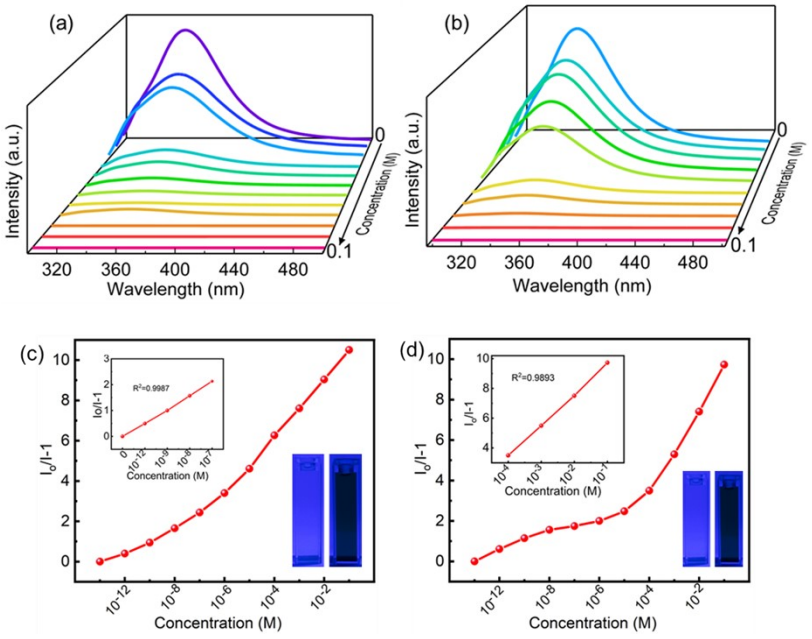


**Fig. S14** Luminescence recognition experiments of NB (a) and NM (b) in $H_2O$. $K_{sv}$ plots of **1** for sensing of NB (c) and NM (d). (Insert: the linear correlation at higher concentrations).

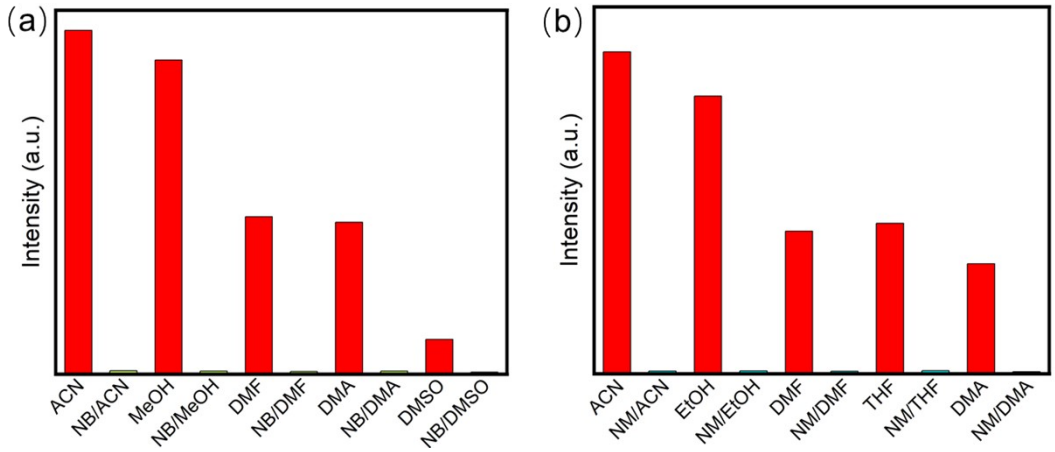


**Fig. S15** The effect of adding other organic solvents on the luminescence intensity of NB and NM.

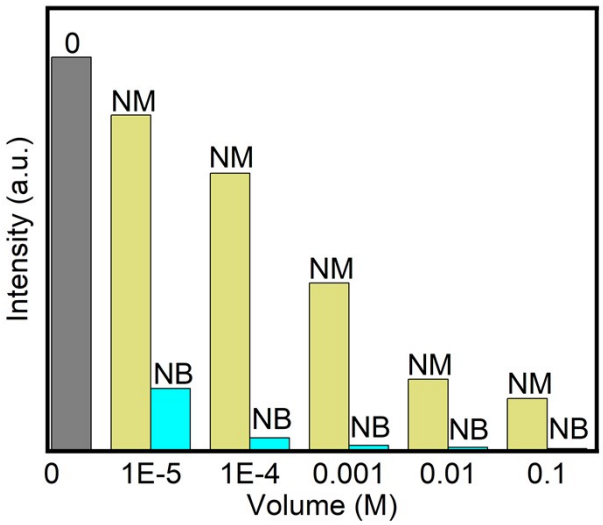


**Fig. S16** Fluorescence spectra of competitive quenching of $Fe^{3+}$ and $Mg^{2+}$.

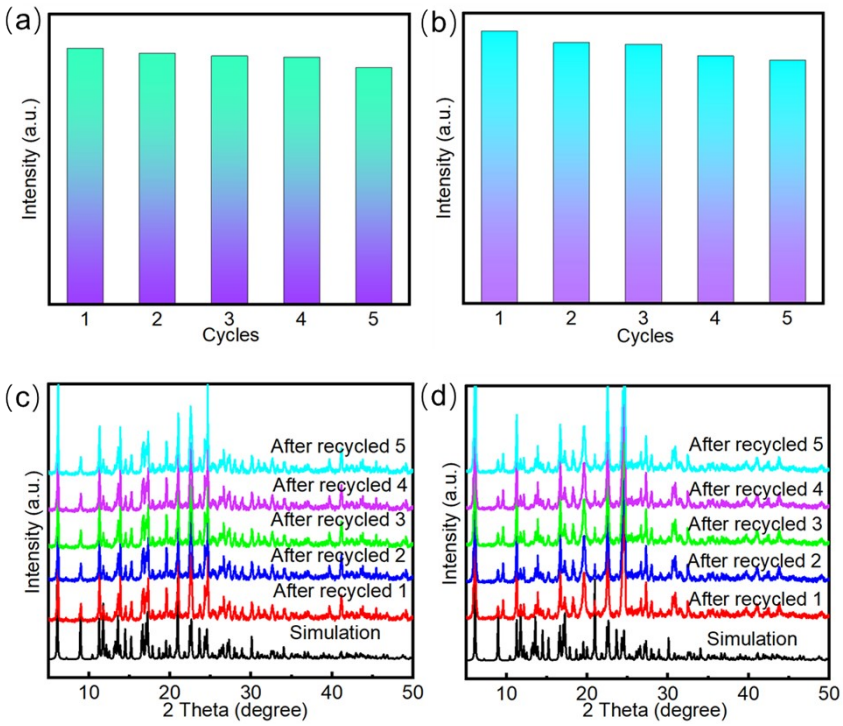


**Fig. S17** The cyclic response of the luminescence intensities of **1** for detecting NB (a) and NM (b). The PXRD patterns of **1** treated by the NB(c), and NM (d)

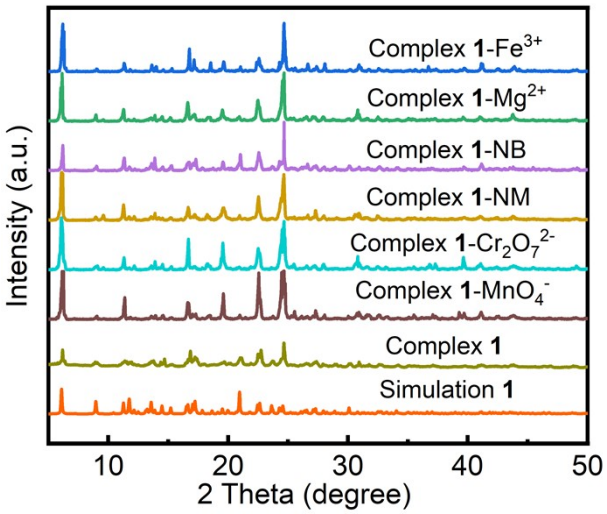


**Fig. S18** The PXRD patterns of **1** before and after exposure to different analyzes.

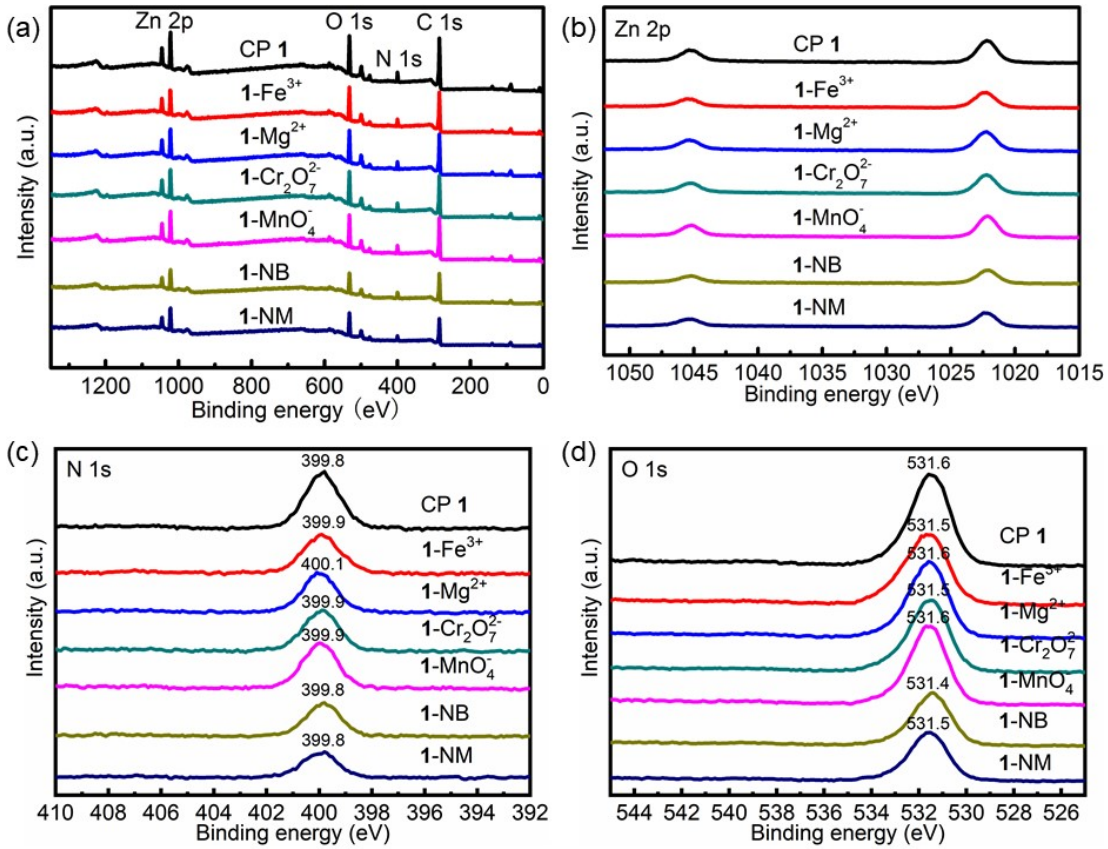


**Fig. S19** XPS spectra of CP **1**, **1**-$Fe^{3+}$, **1**-$Mg^{2+}$, **1**-$Cr_2O_7^{2-}$, **1**-$MnO_4^-$, **1**-NB and **1**-NM. XPS analysis of the Zn2p (b), N1s (c) and O1s (d) spectra of different samples.

**References:**

S1 H. K. Sadhanala, S. Pagidi and A. Gedanken, *J. Mater. Chem. C*, 2021, **9**, 1632–1640.

S2 Z. Fu, J. Qin, Y. Wang, Y. Peng, Y. Zhang, D. Zhao and Z. Zhang, *Dyes Pigments*, 2021, **185**, 108896.

S3 J. Qin, M. Wang, Z. Fu and Z. Zhang, *J. Photoch Photobio*, 2021, **405**, 112965.

S4 X. Wang, Y. Wang, X. Wang, K. Lu, W. Jiang, P. P. Cui, H. Hao and F. Dai, *Dalton Trans*, 2020, **49**, 15473–15480.

S5 J. Ma, N. Xu, Y. Liu, Y. Wang, H. Li, G. Liu, X. Wang and J. Li, *Inorg Chem*, 2020, **59**, 15495–15503.

S6 T. W. T. Wiwasuku, J. B. J. Boonmak, K. S. K. Siriwong, V. E. V. Ervithayasuporn and S. Y. S. Youngme, *Sensor Actuat B-Chem.*, 2019, **284**, 403-413.

S7 R. Lv, J. Wang, Y. Zhang, H. Li, L. Yang, S. Liao, W. Gu and X. Liu, *J. Mater.*

*Chem. A*, 2016, **4**, 15494–15500.

S8 X. Wang, D. Feng, J. Tang, Y. Zhao, J. Li, J. Yang, C. K. Kim and F. Su, *Dalton Trans.*, 2019, **48**, 16776–16785.

S9 X. Y. Guo, Z. P. Dong, F. Zhao, Z. L. Liu and Y. Q. Wang, *New J. Chem.*, 2019, **43**, 2353–2361.

S10 K. S. Asha, K. Bhattacharyya and S. Mandal, *J. Mater. Chem.. C*, 2014, **2**, 10073–10081.

S11 V. M. Suresh, S. J. George and T. K. Maji, *Adv. Funct. Mater.*, 2013, **23**, 5585–5590.

S12 A. Khatun, D. K. Panda, N. Sayresmith, M. G. Walter and S. Saha, *Inorg. Chem.*, 2019, **58**, 12707–12715.

S13 K. Siriwong, V. E. V. Ervithayasuporn and S. Y. S. Youngme, *Sensor Actuat. B*, 2019, **284**, 403–413.

S14 R. Goswami, S. C. Mandal, B. Pathak and S. Neogi, *ACS Appl. Mater. Interfaces*, 2019, **11**, 9042–9053.

S15 X. Wang, D. Feng, J. Tang, Y. Zhao, J. Li, J. Yang, C. K. Kim and F. Su, *Dalton Trans.*, 2019, **48**, 16776–16785.

S16 H. Fu, L. Yan, N. Wu, L. Ma and S. Zang, *J. Mater. Chem. A*, 2018, **6**, 9183–9191.

S17 C. Gogoi, M. Yousufuddin and S. Biswas, *Dalton Trans.*, 2019, **48**, 1766–1773.

S18 X. Zhang, X. Luo, N. Zhang, J. Wu and Y. Huang, *Inorg. Chem. Front.*, 2017, **4**, 1888–1894.

S19 X. Zhang, S. Li, S. Chen, F. Feng, J. Bai and J. Li, *Ecotox. Environ. Safe*, 2020, **187**, 109821.

S20 G. Ji, X. Gao, T. Zheng, W. Guan, H. Liu and Z. Liu, *Inorg. Chem.*, 2018, **57**, 10525–10532.

S21 X. L. Wang, J. X. Ma, N. Xu, Y. Wang, J. Y. Sun and G. C. Liu, *CrystEngComm*, 2021, **23**, 4760–4766.

S22 J. Ma, N. Xu, Y. Liu, Y. Wang, H. Li, G. Liu, X. Wang and J. Li, *Ionrg. Chem.*, 2020, **59**, 15495–15503.

S23 Y. Zhou, L. Cui, Y. Zhang, Y. Liu and D. Ji, *J. Fluoresc.*, 2020, **30**, 1225–1232.

S24 W. Liu, S. Li, J. Shao and J. Tian, *J. Solid State Chem.*, 2020, **290**, 121580.